J. Phys. B: At. Mol. Opt. Phys. **30** (1997) 3009–3017. Printed in the UK PII: S0953-4075(97)82891-X

A quantal study of the rovibrational excitation of H_2 by H

D R Flower

Physics Department, The University, Durham DH1 3LE, UK

Received 25 March 1997

Abstract. Cross sections and rate coefficients have been computed for rovibrational transitions between and within the four lowest vibrational states of H_2, induced in collisions with H atoms. Our quantal close-coupling calculations are compared with previous classical trajectory Monte Carlo results. At low temperatures, there are large discrepancies, whereas, as the temperature increases, the present and previously computed rate coefficients are found to be in satisfactory agreement.

1. Introduction

Recently, there has been a number of studies of the collisional excitation of H_2 molecules by H atoms. The most complete to date are the quasiclassical trajectory (QCT) Monte Carlo calculations of Mandy and Martin (1993), Martin and Mandy (1995), and Lepp *et al* (1995), who studied rotational and vibrational excitation in reactive and non-reactive collisions between the atom and the molecule. Quantal calculations (Sun and Dalgarno 1994, Flower and Wroe 1996), on the other hand, have been restricted to rotationally inelastic processes only.

The recent revival of interest in H–H_2 scattering is attributable to the astrophysical importance of this process, particularly in photon-dominated regions (PDRs) and in shocked-heated gas in the outflows associated with low-mass star formation (Gredel 1994, 1996). Rovibrational transitions within the electronic ground state of H_2 are observed in emission from these regions of the interstellar medium and may, at least in part, be produced by collisional excitation in hot, tenuous gas.

The spacing of the low-lying vibrational levels of H_2 is approximately 6000 K; it is for collision energies of this order (or higher) that the QCT method may be expected to be reliable for vibrationally inelastic transitions. However, Mandy and Martin (1993) and Lepp *et al* (1995) present rate coefficients for transitions between $v = 0$ and $v = 1$ levels at temperatures as low as 1000 K. At such low energies, quantal calculations are desirable to validate (or otherwise) the QCT results; this is the objective of the present study.

2. Theory and numerical methods

The quantal theory of rovibrationally inelastic, non-reactive atom–molecule scattering is well established (see, for example, Flower 1990). Only a brief outline will be given here, with the emphasis on those aspects which are particular to the present study.

0953-4075/97/133009+09$19.50

The problem reduces to having to solve a set of coupled differential equations for the radial functions, $F(R)$, which take the form

$$\left[-\frac{\mathrm{d}^2}{\mathrm{d}R^2}+\frac{l(l+1)}{R^2}-k_{vj}^2\right]F(vjlJ|R)+2\mu\sum_{v'j'l'}V_J(vjl,v'j'l'|R)F(v'j'l'J|R)=0 \qquad (1)$$

where R is the distance between the atom and the centre of mass of the molecule and μ is the reduced mass. In (1), v and j are the vibrational and rotational quantum numbers of the molecule, l is the atom–molecule relative angular momentum quantum number, and $\boldsymbol{J}=\boldsymbol{j}+\boldsymbol{l}$ is the total angular momentum of the system; k_{vj} is the wavenumber in the centre-of-mass coordinate system, relative to level vj of the molecule. The potential matrix element, $V_J(R)$, may be expressed as

$$V_J(vjl,v'j'l'|R)=\sum_\lambda f_\lambda(jl,j'l';J)y_\lambda(vj,v'j'|R) \qquad (2)$$

where f_λ is a Percival–Seaton coefficient and

$$y_\lambda(vj,v'j'|R)=\int_0^\infty \chi^*(vj|r)v_\lambda(r,R)\chi(v'j'|R)\,\mathrm{d}r \qquad (3)$$

is an integral involving the rovibrational eigenfunctions, $\chi(r)$, and the coefficients $v_\lambda(r,R)$ of the expansion of the interaction potential in terms of Legendre polynomials,

$$V(\boldsymbol{r},\boldsymbol{R})=\sum_\lambda v_\lambda(r,R)P_\lambda(\boldsymbol{r}\cdot\boldsymbol{R}), \qquad (4)$$

where $\boldsymbol{r}$ is the intramolecular vector (internuclear axis). In the case of a homonuclear molecule, such as H_2, only even values of λ contribute to the summation in (4).

Partridge *et al* (1993) computed $v_\lambda(r,R)$ for $0\leqslant\lambda\leqslant 8$ and $1.8\leqslant R\leqslant 8.0\ a_0$ at four values of $r=1.2$, 1.401, 1.449 and 1.7 a_0; 1.401 a_0 is the equilibrium separation and 1.449 a_0 is the expectation value of the internuclear distance in the ground vibrational state, $v=0$. In order to compute the integrals in (3), we have used cubic-spline fits to the r-dependence of $v_\lambda(r,R)$ at a given value of R and have substituted harmonic oscillator eigenfunctions for $\chi(vj|r)$. The first three terms, $\lambda=0$, 2, 4, were retained in the Legendre polynomial expansion. These procedures should yield results of acceptable, if not high, accuracy. We note, for example, that the values of $y_\lambda(vj,v'j'|R)$ computed for the vibrational ground state, $v=v'=0$, are in good agreement with $v_\lambda(r,R)$ at the corresponding expectation value, $r=1.449\ a_0$, as was anticipated.

The coupled differential equations (1) were solved, subject to appropriate boundary conditions, by means of the quantal scattering code of Launay (1977); his programme was amended to include the vibrational degree of freedom. The modifications were validated by test calculations on the prototype He–H_2 system, for which 'benchmark' results are available (Eastes and Secrest 1972, Flower and Kirkpatrick 1982). Excellent agreement, extending to four significant figures, was obtained with these earlier calculations of both partial and integral cross sections for rovibrational transitions between and within the $v=0$ and $v=1$ manifolds.

Calculations were performed for H–H_2 using various basis sets. The energies of the rovibrational levels were taken from Dabrowski (1984). The results presented below for para-H_2 were obtained with an {8, 8, 8, 8} basis, i.e. $j=0$, 2, 4, 6, 8 in $v=0$, 1, 2, 3. Equations (1) separate into two sets, corresponding to even and odd values of the total parity, $(-1)^{j+l}$. For values of the total angular momentum $J\geqslant 8$, these sets comprise 80 and 100 coupled equations. The integral cross sections were obtained by summation over J to convergence. At the highest collision energy considered ($E=60\,000$ K), values of J in

excess of 100 were required in order to converge the cross sections for all transitions. Cross sections were computed at approximately 40 collision energies. Results for ortho-H_2 were obtained with a {9, 9, 9, 7} basis, which gives rise to sets of 91 and 110 coupled equations.

3. Results

In table 1 we present the values of the rate coefficients at three kinetic temperatures, $T = 1000$, 2000, 4500 K, for transitions between levels of the $v = 0$, 1, 2 states of para-H_2. The rate coefficients, $q(T)$, for de-excitation were obtained from the relation

$$q(T) = \left(\frac{8kT}{\pi\mu}\right)^{1/2} \int_0^\infty Q(y) y \mathrm{e}^{-y}\, \mathrm{d}y \tag{5}$$

in which $Q(y)$ is the de-excitation cross section and $y = E/kT$; μ is the reduced mass of the H–H_2 system and E the barycentric collision energy, relative to the initial (upper) level. The integral was evaluated numerically, using a trapezoidal rule on a fine grid of the integration variable, y; $Q(y)$ was generated at the grid points by cubic spline interpolation of its computed values. Rate coefficients for excitation, which complete the matrices of results in table 1, were generated by means of the detailed balance relation

$$(2J+1)q_{J\to J'}(T) = (2J'+1)q_{J'\to J}(T)\exp[-(E_{J'} - E_J)/kT]. \tag{6}$$

The corresponding results for ortho-H_2 can be found in table 2.

Mandy and Martin (1993) tabulated rate coefficients for collisional excitation at the temperatures for which results are given in tables 1 and 2. At the lowest temperature, $T = 1000$ K, the values that we have obtained are much smaller than their non-reactive rate coefficients, and those tabulated by Lepp *et al* (1995), increasingly so with increasing excitation energy. For vibrationally inelastic transitions ($v = 0 \to 1$), the discrepancies approach two orders of magnitude. At $T = 2000$ K, the discrepancies are less, approaching one order of magnitude, and, at $T = 4500$ K, there is generally good agreement between the quantal and the QCT results.

We do not believe that these discrepancies, for vibrationally inelastic transitions at low temperatures, arise from differences in the potentials employed. Indeed, the corresponding results of Lepp *et al* (1995), computed using various potentials, are in much better agreement amongst themselves than with the present, quantal values. Rather, we attribute the disagreement to the progressive failure of the QCT method with decreasing collision energy.

The rate coefficients for vibrationally inelastic transitions that we obtain at low temperatures are smaller than the contributions of reactive scattering, according to the results of Mandy and Martin (1993) and Lepp at al (1995). Reactive scattering is not included in the present calculations. Park and Light (1989), on the other hand, performed quantal calculations of the thermal rate constant for the H–H_2 reaction, and the value that they obtain at $T = 1000$ K (2.0×10^{-12} cm^{3}s^{-1}) is in reasonable agreement with the 'reactive' values of $\sum_{v,J} q(00 \to vJ) = 1.5 \times 10^{-12}$ cm^3 s^{-1} $= \sum_{v,J} q(01 \to vJ)$ computed by Lepp *et al* (1995), using the same interaction potential. However, it should be noted that the main contributions to these summations arise from the vibrational ground state, $v = 0$, and so the agreement between the two calculations does not guarantee the accuracy of the QCT results for $v > 0$.

Flower (1997) computed cross sections for (non-reactive) rotational transitions within the vibrational ground state and hence the corresponding rate coefficients for temperatures $T \leqslant 1000$ K. The effects of coupling to excited vibrational states were neglected. It was

Table 1. Rate coefficients (in units of $cm^3\ s^{-1}$) for rovibrational transitions in para-H_2, induced by H atom collisions. Results are given at three values of the kinetic temperature, T. The values of (v, J) which label the columns denote the initial state, those which label the rows denote the final state. Thus, the upper-right triangle of each matrix refers to collisional de-excitation, the lower left to excitation (obtained using the detailed balance relation, equation (6)). More extensive results are available electronically from the CCP7 server (ftp://ccp7.arm.ac.uk/ccp7/) or directly from the author (david.flower@durham.ac.uk).

	(0, 0)	(0, 2)	(0, 4)	(0, 6)	(0, 8)	(1, 0)	(1, 2)	(1, 4)	(1, 6)	(1, 8)	(2, 0)	(2, 2)	(2, 4)	(2, 6)
$T = 1000$ K														
(0, 0)	2.4D − 09	8.7D − 13	9.0D − 14	1.2D − 14	1.7D − 15	1.2D − 14	4.8D − 15	1.5D − 15	3.8D − 16	1.1D − 16	3.0D − 16	1.9D − 16	8.7D − 17	2.7D − 17
(0, 2)	2.6D − 12	2.3D − 09	1.4D − 12	1.4D − 13	1.6D − 14	3.8D − 14	2.7D − 14	1.3D − 14	4.2D − 15	1.2D − 15	1.5D − 15	1.2D − 15	5.9D − 16	3.2D − 16
(0, 4)	1.5D − 13	7.7D − 13	2.3D − 09	1.5D − 12	1.1D − 13	1.9D − 14	6.6D − 14	5.0D − 14	2.4D − 14	6.2D − 15	2.2D − 15	2.6D − 15	2.3D − 15	1.7D − 15
(0, 6)	4.8D − 15	1.9D − 14	3.7D − 13	2.2D − 09	1.3D − 12	3.6D − 15	2.4D − 14	1.8D − 13	1.1D − 13	2.8D − 14	1.4D − 15	3.7D − 15	6.9D − 15	5.8D − 15
(0, 8)	8.6D − 17	2.7D − 16	3.4D − 15	1.7D − 13	2.3D − 09	4.4D − 16	1.2D − 15	4.1D − 14	4.1D − 13	9.3D − 14	1.6D − 16	1.7D − 15	1.0D − 14	1.2D − 14
(1, 0)	2.9D − 17	3.1D − 17	2.9D − 17	2.3D − 17	2.2D − 17	2.3D − 09	1.8D − 12	2.1D − 13	2.8D − 14	3.6D − 15	3.5D − 14	1.0D − 14	4.8D − 15	1.3D − 15
(1, 2)	3.7D − 17	7.0D − 17	3.1D − 16	4.6D − 16	1.9D − 16	5.7D − 12	2.3D − 09	2.8D − 12	2.8D − 13	3.2D − 14	7.3D − 14	6.1D − 14	2.5D − 14	1.0D − 14
(1, 4)	6.9D − 18	1.9D − 17	1.4D − 16	2.0D − 15	3.8D − 15	3.8D − 13	1.6D − 12	2.3D − 09	2.7D − 12	2.1D − 13	3.1D − 14	1.1D − 13	8.7D − 14	3.8D − 14
(1, 6)	4.6D − 19	1.7D − 18	1.7D − 17	3.2D − 16	9.9D − 15	1.3D − 14	4.4D − 14	7.1D − 13	2.3D − 09	2.2D − 12	4.6D − 15	3.7D − 14	3.1D − 13	1.8D − 13
(1, 8)	1.8D − 20	6.5D − 20	6.2D − 19	1.2D − 17	3.1D − 16	2.4D − 16	7.0D − 16	7.7D − 15	3.1D − 13	2.4D − 09	5.1D − 16	1.2D − 15	7.3D − 14	8.0D − 13
(2, 0)	2.7D − 21	4.5D − 21	1.2D − 20	3.0D − 20	2.9D − 20	1.2D − 16	8.3D − 17	6.0D − 17	3.4D − 17	2.7D − 17	2.3D − 09	2.4D − 12	2.2D − 13	2.3D − 14
(2, 2)	5.4D − 21	1.1D − 20	4.3D − 20	2.6D − 19	9.3D − 19	1.1D − 16	2.2D − 16	6.8D − 16	8.6D − 16	1.9D − 16	7.5D − 12	2.2D − 09	3.4D − 12	2.8D − 13
(2, 4)	1.5D − 21	3.4D − 21	2.4D − 20	3.0D − 19	3.5D − 18	3.3D − 17	5.6D − 17	3.3D − 16	4.5D − 15	7.6D − 15	4.3D − 13	2.1D − 12	2.2D − 09	3.2D − 12
(2, 6)	1.4D − 22	5.3D − 22	5.0D − 21	7.2D − 20	1.2D − 18	2.6D − 18	6.6D − 18	4.1D − 17	7.6D − 16	2.4D − 14	1.3D − 14	5.0D − 14	9.2D − 13	2.3D − 09

Table 1. (Continued)

	(0, 0)	(0, 2)	(0, 4)	(0, 6)	(0, 8)	(1, 0)	(1, 2)	(1, 4)	(1, 6)	(1, 8)	(2, 0)	(2, 2)	(2, 4)	(2, 6)
$T = 2000$ K														
(0, 0)	3.1D − 09	7.4D − 12	9.9D − 13	1.7D − 13	3.6D − 14	2.5D − 13	9.8D − 14	3.0D − 14	6.9D − 15	4.4D − 15	1.4D − 14	5.9D − 15	2.6D − 15	7.8D − 16
(0, 2)	2.9D − 11	3.1D − 09	1.2D − 11	1.7D − 12	2.9D − 13	7.5D − 13	5.8D − 13	2.2D − 13	7.2D − 14	3.5D − 14	5.6D − 14	3.7D − 14	1.5D − 14	6.3D − 15
(0, 4)	3.8D − 12	1.2D − 11	3.1D − 09	1.2D − 11	1.4D − 12	4.2D − 13	8.9D − 13	8.2D − 13	3.4D − 13	1.4D − 13	6.2D − 14	7.7D − 14	4.9D − 14	2.6D − 14
(0, 6)	3.9D − 13	9.8D − 13	7.2D − 12	3.1D − 09	1.1D − 11	9.7D − 14	3.6D − 13	1.6D − 12	1.5D − 12	5.0D − 13	3.3D − 14	7.4D − 14	1.4D − 13	1.0D − 13
(0, 8)	3.3D − 14	6.8D − 14	3.4D − 13	4.3D − 12	3.1D − 09	1.9D − 14	5.4D − 14	4.6D − 13	3.2D − 12	1.1D − 12	9.4D − 15	3.5D − 14	1.6D − 13	2.2D − 13
(1, 0)	1.3D − 14	9.7D − 15	5.4D − 15	2.1D − 15	1.0D − 15	3.1D − 09	1.1D − 11	1.6D − 12	2.6D − 13	4.6D − 14	4.2D − 13	1.1D − 13	3.9D − 14	9.5D − 15
(1, 2)	1.9D − 14	3.0D − 14	4.5D − 14	3.1D − 14	1.1D − 14	4.4D − 11	3.1D − 09	1.7D − 11	2.4D − 12	3.9D − 13	9.4D − 13	7.9D − 13	2.6D − 13	8.5D − 14
(1, 4)	6.0D − 15	1.2D − 14	4.3D − 14	1.4D − 13	1.0D − 13	6.5D − 12	1.8D − 11	3.1D − 09	1.6D − 11	2.0D − 12	4.6D − 13	1.2D − 12	1.1D − 12	3.6D − 13
(1, 6)	8.6D − 16	2.3D − 15	1.1D − 14	7.9D − 14	4.4D − 13	6.4D − 13	1.5D − 12	1.0D − 11	3.1D − 09	1.4D − 11	8.7D − 14	3.7D − 13	2.3D − 12	1.8D − 12
(1, 8)	2.3D − 16	4.8D − 16	2.0D − 15	1.2D − 14	6.3D − 14	5.0D − 14	1.0D − 13	5.3D − 13	6.1D − 12	3.1D − 09	1.6D − 14	5.0D − 14	5.7D − 13	5.4D − 12
(2, 0)	4.1D − 17	4.3D − 17	4.7D − 17	4.3D − 17	3.0D − 17	2.5D − 14	1.4D − 14	6.7D − 15	2.1D − 15	9.0D − 16	3.1D − 09	1.3D − 11	1.4D − 12	1.7D − 13
(2, 2)	6.9D − 17	1.1D − 16	2.4D − 16	3.8D − 16	4.4D − 16	2.7D − 14	4.8D − 14	6.8D − 14	3.5D − 14	1.1D − 14	5.1D − 11	3.0D − 09	1.9D − 11	1.9D − 12
(2, 4)	3.3D − 17	4.8D − 17	1.6D − 16	7.6D − 16	2.1D − 15	9.7D − 15	1.6D − 14	6.6D − 14	2.3D − 13	1.3D − 13	5.9D − 12	2.0D − 11	3.1D − 09	1.7D − 11
(2, 6)	6.3D − 18	1.3D − 17	5.4D − 17	3.6D − 16	1.9D − 15	1.5D − 15	3.5D − 15	1.5D − 14	1.2D − 13	8.1D − 13	4.6D − 13	1.3D − 12	1.1D − 11	3.1D − 09

	(0, 0)	(0, 2)	(0, 4)	(0, 6)	(0, 8)	(1, 0)	(1, 2)	(1, 4)	(1, 6)	(1, 8)	(2, 0)	(2, 2)	(2, 4)	(2, 6)
$T = 4500$ K														
(0, 0)	4.2D − 09	3.2D − 11	5.0D − 12	1.1D − 12	3.8D − 13	5.1D − 12	1.6D − 12	5.2D − 13	1.3D − 13	8.2D − 14	4.5D − 13	2.0D − 13	6.5D − 14	2.0D − 14
(0, 2)	1.4D − 10	4.2D − 09	5.3D − 11	9.2D − 12	2.6D − 12	1.1D − 11	9.8D − 12	3.1D − 12	1.0D − 12	5.6D − 13	1.8D − 12	1.1D − 12	3.8D − 13	1.4D − 13
(0, 4)	3.1D − 11	7.3D − 11	4.2D − 09	5.4D − 11	9.9D − 12	5.7D − 12	1.0D − 11	1.1D − 11	3.5D − 12	2.0D − 12	1.1D − 12	1.8D − 12	1.2D − 12	4.1D − 13
(0, 6)	6.6D − 12	1.2D − 11	5.2D − 11	4.3D − 09	5.3D − 11	1.8D − 12	3.8D − 12	1.3D − 11	1.4D − 11	5.7D − 12	5.5D − 13	9.9D − 13	2.4D − 12	1.4D − 12
(0, 8)	1.8D − 12	2.7D − 12	7.4D − 12	4.1D − 11	4.3D − 09	7.2D − 13	1.3D − 12	4.5D − 12	2.1D − 11	1.1D − 11	2.4D − 13	4.8D − 13	1.5D − 12	3.2D − 12
(1, 0)	1.4D − 12	6.5D − 13	2.5D − 13	7.8D − 14	4.1D − 14	4.1D − 09	3.7D − 11	6.0D − 12	1.2D − 12	3.2D − 13	6.5D − 12	1.6D − 12	4.4D − 13	9.6D − 14
(1, 2)	1.9D − 12	2.6D − 12	2.0D − 12	7.6D − 13	3.3D − 13	1.7D − 10	4.2D − 09	6.1D − 11	9.9D − 12	2.4D − 12	1.2D − 11	1.1D − 11	3.1D − 12	8.6D − 13
(1, 4)	8.6D − 13	1.2D − 12	3.0D − 12	3.7D − 12	1.6D − 12	3.8D − 11	8.5D − 11	4.2D − 09	5.7D − 11	1.0D − 11	5.2D − 12	1.1D − 11	1.3D − 11	3.3D − 12
(1, 6)	2.1D − 13	3.8D − 13	9.3D − 13	3.8D − 12	7.5D − 12	7.2D − 12	1.4D − 11	5.7D − 11	4.2D − 09	5.8D − 11	1.3D − 12	3.4D − 12	1.5D − 11	1.6D − 11
(1, 8)	1.1D − 13	1.7D − 13	4.2D − 13	1.2D − 12	3.2D − 12	1.6D − 12	2.7D − 12	8.1D − 12	4.6D − 11	4.3D − 09	4.9D − 13	1.0D − 12	4.6D − 12	2.9D − 11
(2, 0)	3.4D − 14	3.0D − 14	1.4D − 14	6.9D − 15	3.9D − 15	1.9D − 12	7.4D − 13	2.3D − 13	6.1D − 14	2.8D − 14	4.1D − 09	3.9D − 11	4.7D − 12	6.5D − 13
(2, 2)	6.8D − 14	8.3D − 14	9.9D − 14	5.6D − 14	3.5D − 14	2.1D − 12	3.2D − 12	2.2D − 12	7.0D − 13	2.6D − 13	1.8D − 10	4.2D − 09	5.9D − 11	7.0D − 12
(2, 4)	3.2D − 14	4.1D − 14	9.0D − 14	1.9D − 13	1.6D − 13	8.1D − 13	1.2D − 12	3.7D − 12	4.3D − 12	1.7D − 12	3.0D − 11	8.5D − 11	4.2D − 09	5.5D − 11
(2, 6)	9.7D − 15	1.5D − 14	3.2D − 14	1.2D − 13	3.4D − 13	1.8D − 13	3.5D − 13	9.7D − 13	4.6D − 12	1.1D − 11	4.2D − 12	1.0D − 11	5.6D − 11	4.2D − 09

Table 2. As table 1 but for ortho-H_2.

	(0, 1)	(0, 3)	(0, 5)	(0, 7)	(1, 1)	(1, 3)	(0, 9)	(1, 5)	(1, 7)	(2, 1)	(2, 3)	(1, 9)	(2, 5)	(2, 7)
$T = 1000$ K														
(0, 1)	1.8D − 09	1.2D − 12	1.4D − 13	1.8D − 14	2.3D − 14	9.5D − 15	2.7D − 15	2.9D − 15	7.8D − 16	8.1D − 16	4.4D − 16	2.1D − 16	1.9D − 16	4.9D − 17
(0, 3)	1.2D − 12	2.2D − 09	1.5D − 12	1.4D − 13	4.4D − 14	3.5D − 14	1.5D − 14	1.7D − 14	5.1D − 15	2.0D − 15	1.6D − 15	1.3D − 15	8.4D − 16	3.2D − 16
(0, 5)	4.9D − 14	5.3D − 13	2.3D − 09	1.5D − 12	1.9D − 14	1.1D − 13	1.0D − 13	7.2D − 14	2.9D − 14	2.5D − 15	3.9D − 15	6.2D − 15	3.2D − 15	1.6D − 15
(0, 7)	1.1D − 15	8.2D − 15	2.6D − 13	2.3D − 09	2.0D − 15	3.3D − 14	1.2D − 12	2.7D − 13	1.3D − 13	1.2D − 15	5.6D − 15	2.7D − 14	9.3D − 15	5.5D − 15
(1, 1)	5.8D − 17	1.1D − 16	1.3D − 16	8.5D − 17	2.3D − 09	2.6D − 12	5.6D − 17	3.0D − 13	3.7D − 14	5.6D − 14	2.1D − 14	4.5D − 15	8.6D − 15	1.8D − 15
(1, 3)	2.5D − 17	9.3D − 17	8.0D − 16	1.4D − 15	2.7D − 12	2.2D − 09	3.7D − 16	2.8D − 12	2.5D − 13	7.9D − 14	6.8D − 14	2.4D − 14	3.0D − 14	8.9D − 15
(0, 9)	1.5D − 17	8.5D − 17	1.6D − 15	1.2D − 13	1.3D − 16	7.9D − 16	2.3D − 09	4.6D − 14	5.7D − 13	9.3D − 17	1.8D − 15	9.9D − 14	1.5D − 14	1.2D − 14
(1, 5)	2.9D − 18	1.7D − 17	2.1D − 16	4.6D − 15	1.2D − 13	1.1D − 12	8.2D − 15	2.3D − 09	2.5D − 12	2.9D − 14	1.8D − 13	1.6D − 13	1.2D − 13	3.7D − 14
(1, 7)	1.5D − 19	9.8D − 19	1.6D − 17	4.2D − 16	2.8D − 15	1.8D − 14	1.9D − 14	4.7D − 13	2.3D − 09	2.1D − 15	5.3D − 14	1.9D − 12	5.0D − 13	2.0D − 13
(2, 1)	7.2D − 21	1.8D − 20	6.4D − 20	1.8D − 19	2.0D − 16	2.7D − 16	1.5D − 19	2.6D − 16	9.7D − 17	2.2D − 09	3.3D − 12	5.2D − 17	3.0D − 13	2.9D − 14
(2, 3)	4.3D − 21	1.5D − 20	1.1D − 19	9.1D − 19	8.0D − 17	2.5D − 16	3.1D − 18	1.8D − 15	2.7D − 15	3.6D − 12	2.4D − 09	3.6D − 16	3.4D − 12	2.3D − 13
(1, 9)	4.2D − 21	2.6D − 20	3.6D − 19	9.0D − 18	3.6D − 17	1.9D − 16	3.6D − 16	3.3D − 15	2.0D − 13	1.2D − 16	7.4D − 16	2.4D − 09	8.2D − 14	1.0D − 12
(2, 5)	7.5D − 22	3.4D − 21	3.6D − 20	6.2D − 19	1.4D − 17	4.5D − 17	1.0D − 17	4.8D − 16	1.1D − 14	1.4D − 13	1.4D − 12	1.6D − 14	1.8D − 09	2.9D − 12
(2, 7)	4.1D − 23	2.7D − 22	3.7D − 21	7.7D − 20	6.1D − 19	2.8D − 18	1.9D − 18	3.1D − 17	8.7D − 16	2.7D − 15	2.0D − 14	4.2D − 14	6.0D − 13	2.3D − 09

Table 2. (Continued)

	(0, 1)	(0, 3)	(0, 5)	(0, 7)	(1, 1)	(1, 3)	(0, 9)	(1, 5)	(1, 7)	(2, 1)	(2, 3)	(1, 9)	(2, 5)	(2, 7)
$T = 2000$ K														
(0, 1)	2.7D − 09	1.1D − 11	1.6D − 12	2.8D − 13	5.0D − 13	1.8D − 13	6.0D − 14	5.5D − 14	1.4D − 14	3.0D − 14	1.2D − 14	7.0D − 15	4.9D − 15	1.5D − 15
(0, 3)	1.7D − 11	3.1D − 09	1.2D − 11	1.6D − 12	7.6D − 13	6.7D − 13	2.7D − 13	2.6D − 13	8.6D − 14	6.5D − 14	4.2D − 14	3.2D − 14	1.8D − 14	6.5D − 15
(0, 5)	1.8D − 12	9.1D − 12	3.1D − 09	1.2D − 11	3.4D − 13	1.2D − 12	1.3D − 12	1.0D − 12	3.9D − 13	6.1D − 14	9.8D − 14	1.3D − 13	6.1D − 14	2.4D − 14
(0, 7)	1.5D − 13	5.8D − 13	5.7D − 12	3.1D − 09	6.2D − 14	3.9D − 13	9.7D − 12	2.2D − 12	1.6D − 12	2.7D − 14	9.6D − 14	4.2D − 13	1.7D − 13	8.6D − 14
(1, 1)	2.5D − 14	2.5D − 14	1.5D − 14	5.7D − 15	3.1D − 09	1.7D − 11	2.2D − 15	2.4D − 12	3.9D − 13	7.0D − 13	2.1D − 13	6.0D − 14	7.0D − 14	1.7D − 14
(1, 3)	1.4D − 14	3.5D − 14	8.0D − 14	5.6D − 14	2.6D − 11	3.1D − 09	1.6D − 14	1.7D − 11	2.2D − 12	9.7D − 13	8.9D − 13	2.9D − 13	3.0D − 13	9.1D − 14
(0, 9)	1.1D − 14	3.3D − 14	2.1D − 13	3.3D − 12	8.4D − 15	3.9D − 14	3.1D − 09	4.5D − 13	4.0D − 12	5.2D − 15	3.1D − 14	1.0D − 12	1.8D − 13	1.9D − 13
(1, 5)	3.3D − 15	1.0D − 14	5.5D − 14	2.4D − 13	3.0D − 12	1.3D − 11	1.5D − 13	3.1D − 09	1.5D − 11	3.6D − 13	1.6D − 12	1.5D − 12	1.3D − 12	3.8D − 13
(1, 7)	4.5D − 16	1.7D − 15	1.1D − 14	9.0D − 14	2.4D − 13	8.6D − 13	6.5D − 13	7.6D − 12	3.1D − 09	5.5D − 14	4.2D − 13	1.2D − 11	3.3D − 12	1.8D − 12
(2, 1)	8.9D − 17	1.3D − 16	1.6D − 16	1.5D − 16	4.2D − 14	3.7D − 14	8.2D − 17	1.8D − 14	5.3D − 15	3.0D − 09	1.8D − 11	1.5D − 15	2.0D − 12	2.4D − 13
(2, 3)	5.8D − 17	1.3D − 16	4.1D − 16	8.3D − 16	2.0D − 14	5.4D − 14	7.9D − 16	1.3D − 13	6.5D − 14	2.9D − 11	3.1D − 09	1.2D − 14	1.8D − 11	1.7D − 12
(1, 9)	7.9D − 17	2.4D − 16	1.2D − 15	8.6D − 15	1.4D − 14	4.2D − 14	6.3D − 14	2.8D − 13	4.4D − 12	5.7D − 15	2.9D − 14	3.1D − 09	4.9D − 13	5.6D − 12
(2, 5)	1.9D − 17	4.5D − 17	2.1D − 16	1.2D − 15	5.3D − 15	1.5D − 14	3.7D − 15	8.5D − 14	4.1D − 13	2.6D − 12	1.5D − 11	1.7D − 13	2.9D − 09	1.6D − 11
(2, 7)	3.2D − 18	8.8D − 18	4.3D − 17	3.2D − 16	7.0D − 16	2.4D − 15	2.0D − 15	1.3D − 14	1.2D − 13	1.7D − 13	7.4D − 13	1.0D − 12	8.3D − 12	3.1D − 09

	(0, 1)	(0, 3)	(0, 5)	(0, 7)	(1, 1)	(1, 3)	(0, 9)	(1, 5)	(1, 7)	(2, 1)	(2, 3)	(1, 9)	(2, 5)	(2, 7)
$T = 4500$ K														
(0, 1)	4.1D − 09	4.9D − 11	8.4D − 12	2.0D − 12	8.9D − 12	2.8D − 12	7.1D − 13	9.0D − 13	2.7D − 13	9.7D − 13	3.5D − 13	1.3D − 13	1.1D − 13	4.5D − 14
(0, 3)	9.5D − 11	4.2D − 09	5.4D − 11	9.3D − 12	1.0D − 11	1.0D − 11	2.5D − 12	3.3D − 12	1.2D − 12	1.7D − 12	1.1D − 12	4.9D − 13	3.8D − 13	1.6D − 13
(0, 5)	1.8D − 11	6.1D − 11	4.3D − 09	5.2D − 11	4.3D − 12	1.1D − 11	9.1D − 12	1.2D − 11	3.8D − 12	9.7D − 13	2.0D − 12	1.6D − 12	1.2D − 12	4.2D − 13
(0, 7)	3.8D − 12	9.0D − 12	4.5D − 11	4.3D − 09	1.3D − 12	3.8D − 12	4.9D − 11	1.5D − 11	1.4D − 11	4.4D − 13	1.1D − 12	4.5D − 12	2.7D − 12	1.2D − 12
(1, 1)	2.4D − 12	1.4D − 12	5.2D − 13	1.9D − 13	4.2D − 09	5.7D − 11	8.1D − 14	9.6D − 12	2.0D − 12	1.1D − 11	2.8D − 12	4.5D − 13	7.4D − 13	2.1D − 13
(1, 3)	1.5D − 12	2.7D − 12	2.7D − 12	1.0D − 12	1.1D − 10	4.2D − 09	3.7D − 13	6.0D − 11	9.7D − 12	1.1D − 11	1.2D − 11	1.9D − 12	3.2D − 12	1.0D − 12
(0, 9)	9.4D − 13	1.7D − 12	5.5D − 12	3.5D − 11	4.1D − 13	9.6D − 13	4.3D − 09	4.1D − 12	2.2D − 11	1.4D − 13	3.8D − 13	1.1D − 11	1.5D − 12	2.5D − 12
(1, 5)	5.4D − 13	1.0D − 12	3.2D − 12	4.9D − 12	2.2D − 11	6.9D − 11	1.8D − 12	4.2D − 09	5.5D − 11	3.8D − 12	1.2D − 11	8.1D − 12	1.4D − 11	3.7D − 12
(1, 7)	1.4D − 13	3.2D − 13	9.0D − 13	4.0D − 12	3.9D − 12	9.8D − 12	8.8D − 12	4.8D − 11	4.2D − 09	9.9D − 13	3.5D − 12	4.9D − 11	1.9D − 11	1.6D − 11
(2, 1)	7.3D − 14	6.6D − 14	3.4D − 14	1.8D − 14	3.0D − 12	1.5D − 12	8.2D − 15	4.9D − 13	1.4D − 13	4.2D − 09	5.7D − 11	4.1D − 14	7.0D − 12	1.0D − 12
(2, 3)	5.2D − 14	8.5D − 14	1.4D − 13	8.7D − 14	1.6D − 12	3.4D − 12	4.3D − 14	3.1D − 12	1.0D − 12	1.1D − 10	4.2D − 09	2.3D − 13	5.8D − 11	7.0D − 12
(1, 9)	5.0D − 14	9.7D − 14	2.8D − 13	9.1D − 13	6.5D − 13	1.4D − 12	3.0D − 12	5.2D − 12	3.6D − 11	2.1D − 13	5.8D − 13	4.3D − 09	3.3D − 12	2.5D − 11
(2, 5)	2.0D − 14	3.4D − 14	9.4D − 14	2.5D − 13	4.9D − 13	1.1D − 12	2.0D − 13	4.1D − 12	6.3D − 12	1.6D − 11	6.8D − 11	1.5D − 12	4.1D − 09	5.4D − 11
(2, 7)	7.1D − 15	1.3D − 14	3.0D − 14	1.0D − 13	1.3D − 13	3.1D − 13	2.9D − 13	9.8D − 13	4.7D − 12	2.2D − 12	7.3D − 12	1.0D − 11	4.9D − 11	4.2D − 09

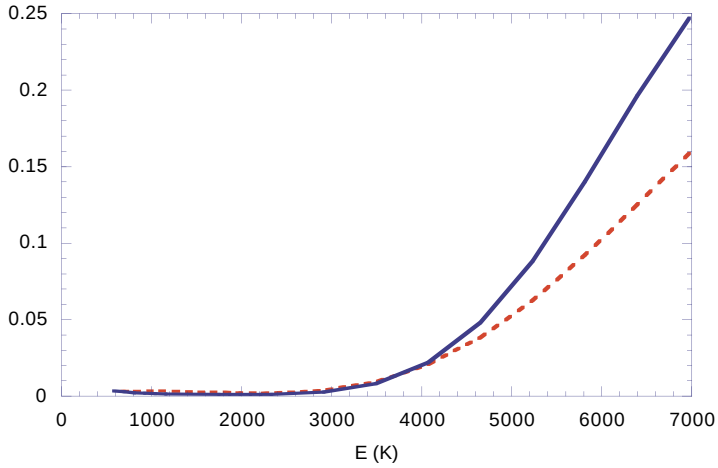

Figure 1. Cross sections for the $(0, 2) \rightarrow (0, 0)$ transition, in units of 10^{-16} cm^2. The centre-of-mass collision energy is expressed in K, relative to the $(0, 0)$ level. Full curve: results obtained including the coupling to vibrationally excited states. Broken curve: results obtained neglecting the vibrational coupling.

shown that, at low collision energies, the potential of Boothroyd *et al* (1991) yields much larger values of the cross sections than the potential of Partridge *et al* (1993), whereas, at energies comparable with the vibrational spacing, the cross sections become very similar. At $T = 1000$ K, the ratios of the rate coefficients computed previously, using the Boothroyd *et al* (1991) potential, to those now obtained from the Partridge *et al* (1993) potential are 1.5 and 1.7 for the $(0, 2) \rightarrow (0, 0)$ and $(0, 3) \rightarrow (0, 1)$ transitions, respectively. For temperatures $T < 1000$ K, the barrier to exchange reactions (about 5000 K: Siegbahn and Liu 1978) should ensure that reactive scattering is unimportant, as is indicated by the calculations of Sun and Dalgarno (1994), which incorporated both reactive and non-reactive scattering.

It is instructive to compare the cross sections for pure rotational transitions with those calculated neglecting the vibrational coupling. In figure 1 we compare the corresponding cross sections for the $(0, 2) \rightarrow (0, 0)$ transition. The effect of including the vibrationally excited channels is to progressively enhance the value of the cross section as the collision energy approaches the vibrational threshold. Similar results are obtained for the $(0, 3) \rightarrow (0, 1)$ transition.

4. Concluding remarks

In the previous section, we showed that the results of quantal and QCT calculations diverge when the collision energy falls below the energetic spacing of the levels involved. The emphasis of the present study has been on vibrationally inelastic transitions. Lepp *et al* (1995), on the other hand, have already shown that quantal and QCT calculations of cross sections, and hence rate coefficients, for pure rotational transitions, $(0, 0)$–$(0, 2)$ and $(0, 1)$–$(0, 3)$, also part company for temperatures approaching the corresponding thresholds. In this case, the quantal results exceed those derived from the QCT method.

Mandy and Martin (1992) have compared their QCT calculations of the cross sections

for the exchange reactions

$$H + H_2(0, j = 0, 2) \rightarrow H_2(1, j' = 1, 3, 5) + H$$

with quantal results. They found satisfactory agreement when the cross sections for these excitation processes were deduced, by means of the detailed balance relation, from those calculated for de-excitation using the QCT method. However, when calculated directly using QCT, the excitation cross sections failed to satisfy detailed balance and were found to fall increasingly above the cross sections deduced from detailed balance, and the quantal values, as threshold was approached. The violation of microscopic reversibility is symptomatic of the failure of the QCT method near threshold.

References

Boothroyd A I, Keogh W J, Martin P G and Peterson M R 1991 *J. Chem. Phys.* **95** 4343
Dabrowski I 1984 *Can. J. Phys.* **62** 1639
Eastes W and Secrest D 1972 *J. Chem. Phys.* **56** 640
Flower D R 1990 *Molecular Collisions in the Interstellar Medium* (Cambridge: Cambridge University Press)
Flower D R 1997 *Mon. Not. R. Astron. Soc.* **288** 627
Flower D R and Kirkpatrick D J 1982 *J. Phys. B: At. Mol. Phys.* **15** 1701
Flower D R and Wroe R A 1996 *J. Phys. B: At. Mol. Opt. Phys.* **29** L851
Gredel R 1994 *Astron. Astrophys.* **292** 580
Gredel R 1996 *Astron. Astrophys.* **305** 582
Launay J-M 1977 *J. Phys. B: At. Mol. Phys.* **10** 3665
Lepp S, Buch V and Dalgarno A 1995 *Astrophys. J. Suppl.* **98** 345
Mandy M E and Martin P G 1992 *J. Chem. Phys.* **97** 265
Mandy M E and Martin P G 1993 *Astrophys. J. Suppl.* **86** 199
Martin P G and Mandy M E 1995 *Astrophys. J.* **455** L89
Park T J and Light J C 1989 *J. Chem. Phys.* **91** 974
Partridge H, Bauschlicher C W, Stallcop J R and Levin E 1993 *J. Chem. Phys.* **99** 5951
Siegbahn P and Liu B 1978 *J. Chem. Phys.* **68** 2457
Sun Y and Dalgarno A 1994 *Astrophys. J.* **427** 1053